ACS APPLIED MATERIALS & INTERFACES

www.acsami.org

Research Article

Understanding the Performance of NiO Photocathodes with Alkyl-Derivatized Cobalt Catalysts and a Push–Pull Dye

Kelly L. Materna, Anna M. Beiler, Anders Thapper, Sascha Ott, Haining Tian, and Leif Hammarström*

Cite This: *ACS Appl. Mater. Interfaces* 2020, 12, 31372–31381

Read Online

ACCESS | Metrics & More | Article Recommendations | Supporting Information

ABSTRACT: Mesoporous NiO photocathodes containing the push–pull dye PB6 and alkyl-derivatized cobaloxime catalysts were prepared using surface amide couplings and analyzed for photocatalytic proton reduction catalysis. The length of the alkyl linker used to derivatize the cobalt catalysts was found to correlate to the photocurrent with the highest photocurrent observed using shorter alkyl linkers but the lowest one for samples without linker. The alkyl linkers were also helpful in slowing dye–NiO charge recombination. Photoelectrochemical measurements and femtosecond transient absorption spectroscopic measurements suggested electron transfer to the surface-immobilized catalysts occurred; however, H_2 evolution was not observed. Based on UV–vis, X-ray fluorescence spectroscopy (XRF), and X-ray photoelectron spectroscopy (XPS) measurements, the cobalt catalyst appeared to be limiting the photocathode performance mainly via cobalt demetallation from the oxime ligand. This study highlights the need for a deeper understanding of the effect of catalyst molecular design on photocathode performance.

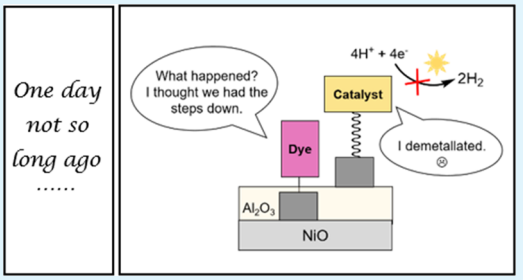

KEYWORDS: *solar fuels, photocathode, nickel oxide, cobalt, cobaloxime*

INTRODUCTION

Since climate change is actively occurring, fossil fuels must be replaced by clean, renewable fuels.[1] Water-splitting dye-sensitized photoelectrochemical cells (WS-DSPECs) have been proposed as one way to meet this demand for clean fuels.[2−6] WS-DSPECs work by mimicking the processes occurring in natural photosynthesis by performing water oxidation catalysis (on the photoanode) in tandem with fuel forming reactions (on the photocathode). Here, we will focus on the photocathode component with the goal to produce H_2 gas as a renewable fuel.

Photocathodes in WS-DSPECs contain both molecular dyes to harvest sunlight and molecular proton reduction catalysts to perform hydrogen evolution catalysis.[7−9] Both molecules are immobilized on a semiconductor electrode (usually NiO), commonly by a covalent linkage using surface anchoring groups (carboxylic acids, phosphonic acids, hydroxamic acids, silatranes), which are already attached to the molecules. To operate, the photocathode is illuminated, which causes the dye to become photoexcited and inject a hole into the NiO valence band, generating the reduced dye. The reduced dye can then reduce a nearby catalyst molecule, initiating proton reduction catalysis once the catalyst gains enough reducing equivalents and protons. This is quite challenging, as all of these processes must occur faster than unwanted charge recombination to function efficiently.[7,8]

To date, tandem WS-DSPECs have exhibited poor overall performance primarily because the photocathodes have performed poorly compared to the photoanode despite a multitude of tested photocathode strategies and architectures.[7−11] Some strategies for photocathode assemblies have included codeposition of dye and catalyst,[10,12−16] covalently linking dye and catalyst,[17−20] layer-by-layer strategies,[21−23] adding hydrophobic or electron shuttling layers,[24,25] atomic layer deposition,[26] and supramolecular assemblies.[27] In addition, we have recently developed a surface amide coupling procedure for photocathode assembly where dye or catalyst molecules containing carboxylic acid functional groups can be amide-coupled to amine-derivatized surface-immobilized groups to easily tune and screen a variety of photocathode architectures.[14]

In many cases, efficient catalysis on photocathodes is difficult because charge recombination processes are faster than the charge accumulation at the catalyst needed for turnover to occur.[12,22,23,28−34] To help slow down charge recombination, some strategies can be employed to increase the catalytic efficiency. A strategy that has shown promise involves putting the surface-bound dye on the electrode in a hydrophobic environment such as by surrounding the dye with long alkyl chains either codeposited or included as a part of the molecular structure.[24,35] This has been shown to slow down

Received: March 20, 2020
Accepted: June 15, 2020
Published: June 15, 2020

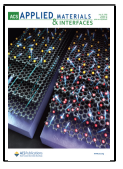

https://dx.doi.org/10.1021/acsami.0c05228
ACS Appl. Mater. Interfaces 2020, 12, 31372–31381

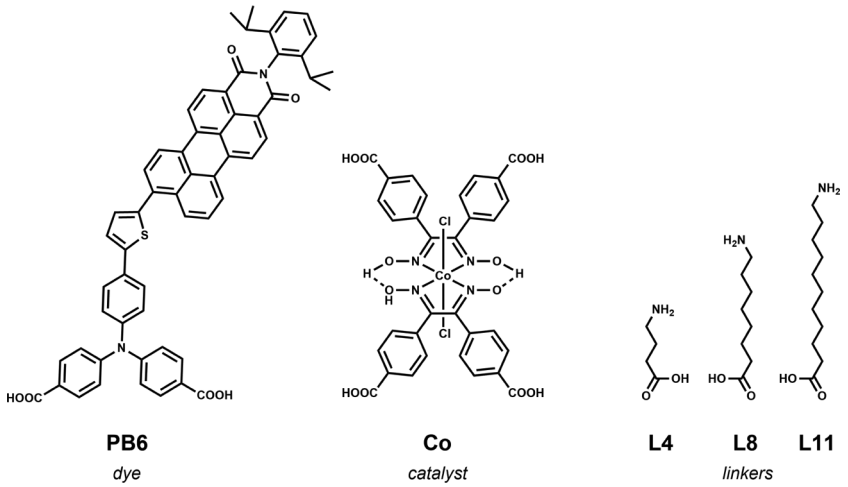

Figure 1. Molecular structures of **PB6** dye; **Co** proton reduction catalyst; and **L4**, **L8**, and **L11** alkyl linkers to be used in the study. The amine of the linkers was amide-coupled to the carboxylic acid of **Co** during electrode preparation.

dye−NiO charge recombination with ruthenium dyes[35] and has also been applied in photocathodes with a Mo−S cluster proton reduction catalyst and a push−pull dye.[24] In addition, covering the NiO and/or encasing the dye with an insulating material, such as Al_2O_3, via atomic layer deposition (ALD) can aid in slowing dye−NiO charge recombination; this strategy has been applied in both the photocathode and photoanode field.[26,36−40] Using these strategies, one can produce a photocathode with a greater chance of performing catalysis.

Recently, we have studied the dye **PB6** (Figure 1) for use in NiO-based photocathodes (Figure 1).[14,25,41,42] **PB6** is known to perform ultrafast hole injection (<300 fs) upon photoexcitation and generate the reduced state **PB6**$^-$ (−0.93 V vs normal hydrogen electrode (NHE) for **PB6**/**PB6**$^-$),[41] which is at a potential capable of reducing many proton reduction catalysts. We have also studied the photoelectrochemical performance of NiO-**PB6** photocathodes, which show excellent long-term photoelectrochemical stability in aqueous conditions.[14] In separate studies, we found that **PB6** is stable under ALD preparation conditions and demonstrated that using ALD of Al_2O_3 and/or TiO_2 can slow charge recombination on NiO-**PB6** electrodes in a variety of assemblies.[41−43] Furthermore, ALD is a useful technique as it can be used to build a platform for immobilizing a catalyst further from the metal oxide surface or dye.[44] As an added benefit, ALD has been shown to increase a dye's photostability and decrease dye desorption from the electrode.[26,36,39,45]

Molecular catalysts based on cobalt, nickel, or iron are the most commonly studied earth-abundant compounds for electrocatalytic proton reduction and have also been applied as catalysts in photoelectrocatalysis by immobilization on photocathodes.[7,8,43,46] For example, cobaloxime catalysts have shown promise in electrocatalysis[43,46−49] and have been immobilized onto photocathodes for photocatalytic proton reduction catalysis using different types of assemblies.[13,17,50−53] Recently, a new cobaloxime catalyst, **Co** (Figure 1), has been shown to be active for electrocatalytic proton reduction (−0.45 V vs RHE) when incorporated into a surface-immobilized metal−organic framework (MOF).[54] In this MOF, **Co** performed more than 20000 turnovers under aqueous conditions with no loss in current over 18 h of operation. Since it had good stability on the electrode, it has the potential to be applied in a photocathode.

Thus, here we report the assembly of photocathodes with **PB6** incorporating ALD of Al_2O_3 in an attempt to slow charge recombination and provide a platform for surface-immobilized catalysts. Alkyl-linked **Co** catalysts are used to provide a hydrophobic environment around **PB6** with the aim to further slow charge recombination, and surface amide couplings are used to prepare alkyl **Co** catalysts for easy tunability.

RESULTS AND DISCUSSION

Assembly Rationale. In the photocathodes studied herein, we use **PB6** as the dye molecule and **Co** as the catalyst molecule on the electrodes (Figure 1). As stated above, **PB6** is capable of hole injection into the NiO valence band upon photoexcitation with the resulting **PB6**$^-$ possessing enough driving force to reduce the **Co** catalyst.[41] Electrodes were assembled in the architecture depicted in Figure 2. In this

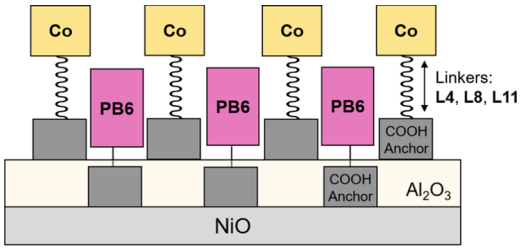

Figure 2. Photocathode architectures prepared using alkyl-linked catalysts. **PB6** is first bound to the NiO substrate, followed by 0.2 nm of Al_2O_3 applied by atomic layer deposition (ALD). The linkers are then bound to the Al_2O_3 layer and **Co** subsequently attached via a surface amide coupling to the amine on the surface-bound linker.

architecture, **PB6** is partially covered by Al_2O_3 using ALD. ALD of Al_2O_3 was chosen for several reasons: (1) it may slow NiO−dye charge recombination;[26,37,40] (2) it can be used as an anchoring platform to subsequently immobilize **Co** on the electrode and so separate **Co** further from NiO, which theoretically will slow **Co**−NiO charge recombination;[44] and (3) it could also enhance dye photostability and hinder desorption.[26,39,45] Alkyl linkers (**L4**, **L8**, or **L11**; Figure 1) with varying lengths are attached to the Al_2O_3 via their carboxylic acid anchoring groups, providing a hydrophobic environment around **PB6**, which also aims to slow dye−NiO charge

https://dx.doi.org/10.1021/acsami.0c05228
ACS Appl. Mater. Interfaces 2020, 12, 31372−31381

recombination.[35] Co is then attached to the linkers via a surface amide coupling procedure we recently developed via coupling of the carboxylic acids of **Co** with the amine of the linkers to create a surface amide bond.[14] The linkers and Al_2O_3 layer help separate **Co** further from the NiO surface (which could help slow **Co**−NiO and **Co**−**PB6** charge recombination). The different linkers also place **Co** at varying distances from **PB6**. Distance between dye and catalyst could change performance as electron transfer kinetics are distance-dependent;[22,23] thus, it is important to investigate which linker gives the best performance.

Electrode Preparation. NiO thin films were prepared by screen-printing NiO paste onto fluorine-doped tin oxide (FTO)-coated glass electrodes (see the Supporting Information, SI, for more details). The NiO electrodes were next soaked in a 0.2 mM 1:1 dichloromethane/methanol solution of **PB6** for 50 min, rinsed, and air-dried, resulting in NiO-**PB6** electrodes; this gave a **PB6** surface coverage of ~35 nmol/cm^2 (76% of a monolayer, Figure S4) as found by UV−vis spectroscopy, providing free space on the surface for the linker molecules to bind later (Scheme 1, step 1). Next, ALD of

Scheme 1. Electrode Assembly Process: (1) PB6 Sensitization, (2) ALD of Al_2O_3, (3) Alkyl Linker, (L4, L8, or L11) Electrode Sensitization, and (4) Co Immobilization via a Surface Amide Coupling Procedure

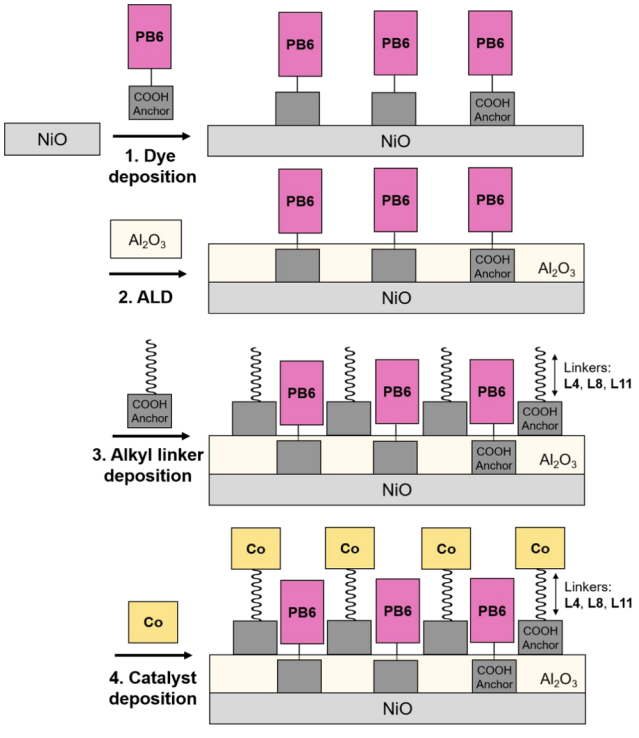

Al_2O_3 was performed at 300 °C in the presence of trimethylaluminum, giving a ~0.2 nm layer of Al_2O_3 over the **PB6**, producing NiO-**PB6**-Al_2O_3 electrodes (Scheme 1, step 2). Next, the linkers (**L4**, **L8**, or **L11**) were bound to the Al_2O_3 surface by soaking NiO-**PB6**-Al_2O_3 in a 4 mM solution of either **L4**, **L8**, or **L11** overnight (Scheme 1, step 3). Post sensitization, the electrodes were rinsed and air-dried, resulting in NiO-**PB6**-Al_2O_3-**L4**, NiO-**PB6**-Al_2O_3-**L8**, or NiO-**PB6**-Al_2O_3-**L11** electrodes. Finally, a surface amide coupling procedure was performed to attach **Co** to the electrodes by soaking the linker-functionalized electrodes overnight in 0.1 mM **Co** methanol solution containing 1 mM 1-ethyl-3-(3-dimethylaminopropyl)carbodiimide (EDC) as an amide coupling agent (Scheme 1, step 4).[14] Post sensitization, electrodes were rinsed and air-dried affording NiO-**PB6**-Al_2O_3-**L4**-**Co**, NiO-**PB6**-Al_2O_3-**L8**-**Co**, or NiO-**PB6**-Al_2O_3-**L11**-**Co** electrodes. A control sample without linker was also prepared by soaking NiO-**PB6**-Al_2O_3 in a 0.1 mM methanol **Co** solution overnight, affording NiO-**PB6**-Al_2O_3-**Co** electrodes. Further details on the electrode preparation method can be found in the Supporting Information (SI).

Electrode Characterization. As we have previously observed, UV−vis spectroscopic measurements of the NiO-**PB6** electrodes show a signature peak at 530 nm, indicative of **PB6** binding to the electrode (Figure 3A).[14,25,41,42] This

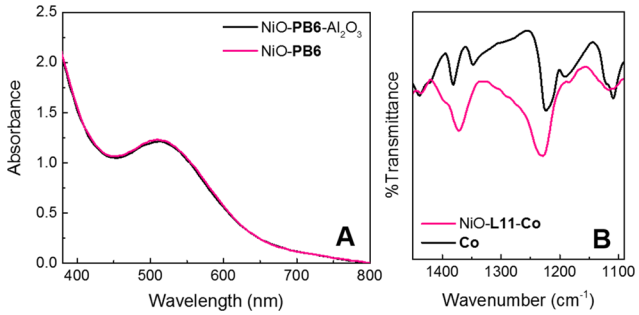

Figure 3. (A) UV−vis spectra of NiO-**PB6** (pink) and NiO-**PB6**-Al_2O_3 (black). (B) Attenuated total reflection Fourier-transform infrared (ATR-FTIR) spectra of **Co** catalyst powder (black) and NiO-**L11**-**Co** (pink).

feature also matches well with the UV−vis of **PB6**, suggesting that the molecular structure is retained upon binding to the electrode surface (Figure S3). Post ALD of Al_2O_3, the UV−vis spectrum of NiO-**PB6**-Al_2O_3 does not change compared to NiO-**PB6**, strongly supporting the good stability of **PB6** at the high-temperature ALD conditions (Figure 3A). The electrodes with linker and catalyst molecules have UV−vis spectra similar to NiO-**PB6**-Al_2O_3 (Figures S6 and S7). This is expected as the UV signatures of the linkers are screened by NiO scattering below 400 nm (Figure S8) and the relatively large extinction coefficient of **PB6** masks the expected features of **Co** (Figures S3 and S8).

To gain evidence for **Co** immobilization onto the electrode via amide coupling, X-ray fluorescence (XRF) spectroscopy was used to assess if cobalt was present on the electrodes. Indeed, all samples with **Co** (NiO-**PB6**-Al_2O_3-**L4**-**Co**, NiO-**PB6**-Al_2O_3-**L8**-**Co**, NiO-**PB6**-Al_2O_3-**L11**-**Co**, or NiO-**PB6**-Al_2O_3-**Co**) were found by XRF to have cobalt, confirming immobilization of **Co** onto the electrodes, while control samples not exposed to **Co** lacked cobalt (Table S1). To obtain **Co** loadings, an XRF calibration curve was constructed using electrodes with known **Co** loadings prepared by drop-casting **Co** on the electrodes (Figure S2). Using this calibration curve, the **Co** loadings on all photocathodes were found to be ~15−16 nmol/cm^2.

To determine if the linker/**Co** amide couplings had occurred, octanoic acid, a CH_3-terminated alkyl linker (Figure S1), was bound to the NiO-**PB6**-Al_2O_3 electrodes (see the SI for preparation details). Since there is no amine present in octanoic acid, no amide coupling should occur, and thus no **Co** should bind to the electrode. In addition, if the octanoic acid

https://dx.doi.org/10.1021/acsami.0c05228
ACS Appl. Mater. Interfaces 2020, 12, 31372−31381

linkers have saturated the surface, then **Co** should not bind since there will not be any free surface sites available on the Al_2O_3 layer. To test this, an amide coupling procedure was performed by exposing the NiO-**PB6**-Al_2O_3−octanoic acid electrode to a **Co**/EDC solution overnight, as described above. Insignificant loadings of **Co** were found on the electrode (3 nmol/cm^2 compared the ca. 15−16 nmol/cm^2 observed for electrodes with amines present), which strongly suggests that the amide coupling occurs only when the amine-derivatized linkers are bound to the electrode surface; the small quantity of **Co** found on the NiO-**PB6**-Al_2O_3−octanoic acid electrodes likely results from **Co** binding to the remaining free surface sites not blocked by **PB6** or the alkyl linkers. This control also indirectly suggests that the linkers are bound to Al_2O_3, blocking the majority of remaining surface sites. In addition, this control further supports that **Co** does not displace the linkers on the surface during the amide coupling procedure. Contrastingly, when no linkers are present on the surface (i.e., NiO-**PB6**-Al_2O_3-**Co**), **Co** can bind to the electrode in higher amounts (∼19 nmol/cm^2), presumably in empty surface sites not occupied by **PB6** molecules. Finally, ATR-FTIR measurements showed a diagnostic feature at 1225 cm^{-1} for the N−O$^-$ stretch of the oxime ligand (Figures 3B and S13).[55] This was observed for both **Co** catalyst powder and surface-immobilized **Co** strongly supporting that the molecular structure is retained upon binding to the electrode. In addition, X-ray photoelectron spectroscopy (XPS) measurements displayed a clear peak in the N 1s region, also supporting the presence of the oxime ligand on the surface (Figure S14). One should note that **PB6** also contains N and thus has a peak in the N 1s region; however, when **Co** is added to the electrodes, the N 1s signal significantly grows, which further suggests the binding of **Co** to the electrodes. Taken together, the octanoic acid control experiments as well as XRF, ATR-FTIR, and XPS measurements support that **Co** is successfully immobilized on the electrode surface via an amide coupling to the preimmobilized linkers **L4**, **L8**, and **L11**.

Photoelectrochemistry. To test if the photocathodes could produce photocurrent upon illumination, photoelectrochemical measurements were performed. First, chronoamperometric (CA) measurements were performed on the **PB6**-only samples in 0.1 M 2-(*N*-morpholino)ethanesulfonic acid (MES) buffer at pH 5 with a 0.1 V vs NHE bias. Similar to what we previously observed with **PB6**-based photocathodes, all samples showed a response to light resulting in stable photocurrent (Figure S17).[25,29] This indicates that upon photoexcitation, **PB6** subsequently injects a hole into the NiO valence band.

When **Co** is immobilized on the electrode, all samples showed an increase in photocurrent upon illumination, which was significantly larger compared to the samples without **Co** (Figures 4A, S17, and S18). Since **PB6**$^-$ (−0.93 V vs NHE for **PB6**/**PB6**$^-$) should theoretically be able to reduce **Co** (−0.45 V vs RHE) on the electrode, the larger photocurrent with the catalyst present suggests that **PB6**$^-$ can reduce **Co** at least once (Figures 4, S17, and S18). In addition, control samples of bare NiO, NiO-**L4**, NiO-**L8**, NiO-**L11**, NiO-**Co**, NiO-**L4**-**Co**, NiO-**L8**-**Co**, and NiO-**L11**-**Co** did not generate significant photocurrent, supporting that the photocurrent generated from electrodes with both **PB6** and **Co** should be from **Co** reduction and/or catalysis (Figure S19).

Interestingly, a reproducible trend in photocurrent was observed in **Co** containing electrodes depending on the linker

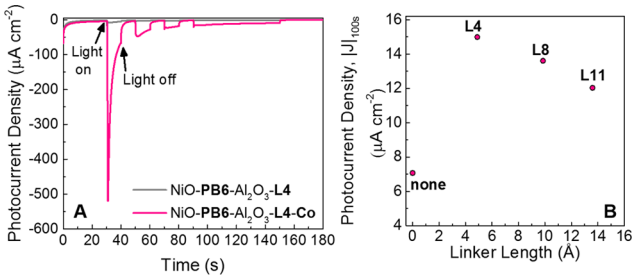

Figure 4. (A) Chopped light chronoamperograms of NiO-**PB6**-Al_2O_3-**L4** (gray) and NiO-**PB6**-Al_2O_3-**L4**-**Co** (pink) in 0.1 M MES buffer at pH 5 with an applied potential of 0.1 V vs NHE. The photocathodes were illuminated from 30 to 40, 50 to 60, 70 to 80, and 90 to 150 s. (B) Photocurrent trend with linker length. The linker length was estimated by measuring the distance from the carbon of the carboxylic acid to the nitrogen atom of the amine in Chem3D. The photocurrent density after 100 s of illumination is shown for NiO-**PB6**-Al_2O_3-**Co** (no linker, labeled "none"), NiO-**PB6**-Al_2O_3-**L4**-**Co** (L4), NiO-**PB6**-Al_2O_3-**L8**-**Co** (L8), and NiO-**PB6**-Al_2O_3-**L11**-**Co** (L11).

used (Figure 4B). Electrodes with the **L4** linker (NiO-**PB6**-Al_2O_3-**L4**-**Co**) generated the highest photocurrents, but when the longer **L8** and **L11** linkers were used, the photocurrents decreased as the linker length increased. Presumably, as the **Co** catalyst gets further from **PB6**, it is harder to transfer an electron to the **Co** catalyst, and thus the photocurrent decreases. Interestingly, without a linker (NiO-**PB6**-Al_2O_3-**Co**), the currents were the lowest of all samples. This may suggest that **Co**−NiO charge recombination is too fast for the charge to build up at the **Co** center. Charge recombination could be fast if **Co** is too close to the NiO surface without the benefit of the surface alkyl linkers, which would slow charge recombination when present. Therefore, the use of surface alkyl linkers on these photocathodes is necessary to provide higher photocurrents by possibly slowing **PB6**−NiO charge recombination. The **L4** linker gave an optimal architecture where **Co** is slightly distanced from **PB6** and NiO, allowing it to receive an electron from **PB6**$^-$ while possibly slowing **Co**−NiO charge recombination. Clearly, small molecular changes on an electrode surface can provide noticeable changes in photocurrents. One should note that due to the inherent heterogeneity of the films, some differences in photocurrent magnitudes occurred between batches prepared on separate occasions. However, the overall trend in photocurrent with linker length was reproducible for each batch of samples prepared at the same time. To minimize errors when comparing samples, care was taken to prepare a full set of samples using the same sensitization conditions starting on the same day. Since the use of the **L4** linker provided samples with the highest photocurrents, we will only use these electrodes hereafter.

Ultrafast Electron Transfer Dynamics. Since the NiO-**PB6**-Al_2O_3-**L4**-**Co** electrodes showed promising photocurrent responses, we wanted to further understand the charge transfer dynamics on the surface. To do this, femtosecond transient absorption spectroscopy (fsTAS) was performed on dry photocathodes in air. The simplest electrode, NiO-**PB6**, was first analyzed. NiO-**PB6** was photoexcited at 560 nm, resulting in transient spectra displaying a negative ground-state bleach at 530 nm, a positive absorption at > 650 nm, and stimulated emission at 620 nm (Figure 5A) similar to what we have previously observed with NiO-**PB6** films.[14,41,42] Global analysis

https://dx.doi.org/10.1021/acsami.0c05228
ACS Appl. Mater. Interfaces 2020, 12, 31372−31381

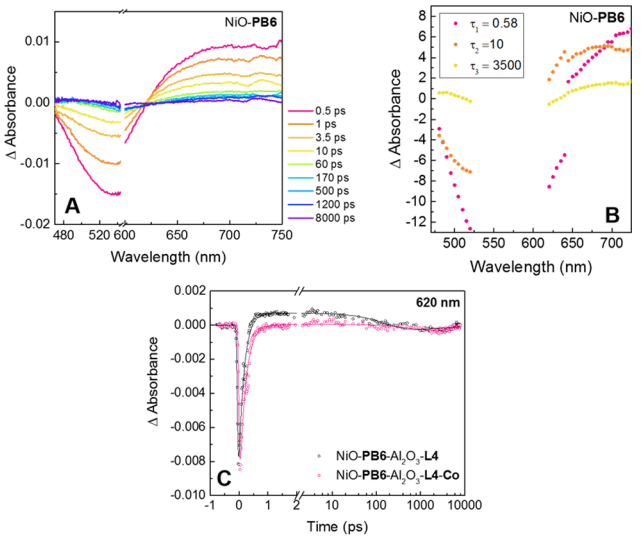

Figure 5. (A) Transient absorption spectra of NiO-**PB6** with photoexcitation at 560 nm. (B) Decay associated spectra of NiO-**PB6**; time constants, (pink) τ_1, (orange) τ_2, and (yellow) τ_3, have units of ps. (C) Kinetic traces at 620 nm for NiO-**PB6**-Al_2O_3-**L4** (black) and NiO-**PB6**-Al_2O_3-**L4**-**Co** (pink).

was performed by fitting the data to a triple exponential function resulting in the following lifetimes: τ_1 = 0.58 ps, τ_2 = 10 ps, and τ_3 = 3500 ps (Table 1). Hole injection from **PB6*** into the NiO valence band likely corresponds to the first time component (τ_1), which generates the **PB6**$^-$ reduced state.[14,41] The second (τ_2) and third (τ_3) slower time components are likely attributed to charge recombination between **PB6**$^-$ and NiO(+).[14,41]

Table 1. Results from Global Analysis from Fitting to a Triple Exponential Function[a]

sample	τ_0 (ps)	IRF (ps)	τ_1 (ps)	τ_2 (ps)	τ_3 (ps)
NiO-**PB6**	0.09	0.19	0.58	10	3500
NiO-**PB6**-Al_2O_3	0.10	0.16	0.50	9.3	3900
NiO-**PB6**-Al_2O_3-**L4**	0.10	0.19	0.47	11	5500
NiO-**PB6**-Al_2O_3-**L4**-**Co**	0.09	0.17	0.48	9.1	4600

[a]IRF is the width of instrument response function (full width at half-maximum), τ_0 is time zero, and τ_{1-3} is the first, second, and third time components, respectively.

Stimulated emission from **PB6*** can be followed in the kinetic traces at 620 nm showing an instrument-limited bleach followed by a growth of a positive signal (τ_1 = 0.58 ps) and decay to baseline (~1 ns, represented by τ_2 and τ_3). This trace suggests the formation of at least one intermediate upon excitation and is in good agreement with the formation of the charge-separated state, NiO(+) and **PB6**$^-$.[14,41,42] Furthermore, the formation of the charge-separated state can be followed through the 620 nm trace, where we see the formation of **PB6*** (initial negative signal), formation of **PB6**$^-$ (positive signal), and decay to the ground state via charge recombination (positive signal returns to baseline). The positive signal in the 620 nm kinetic trace is less pronounced than our previous work[14] likely due to the lower loading of **PB6** on the electrodes in this study.

Furthermore, decay associated spectra support the generation of **PB6*** and **PB6**$^-$ on the electrodes (Figure 5B); the first time component (τ_1) matches the characteristic difference spectra of **PB6*** (minus the ground state), while the second (τ_2) and third (τ_3) time components show spectra that correspond to the difference spectrum of **PB6**$^-$ consistent with our prior work.[14,41,42] One should note that since photocathode surfaces have an inherent heterogeneity, injection and recombination processes may overlap on different timescales and the time components could include multiple overlapping processes.[32,56]

Next, the effect of ALD, alkyl linker, and catalyst on the photocathode architecture was analyzed. When ALD of Al_2O_3 was added to the photocathode in NiO-**PB6**-Al_2O_3, similar transient absorption spectra and decay associated spectra were observed compared to the photocathode lacking Al_2O_3 (Figures S23 and S24). With Al_2O_3, a slower NiO(+)−**PB6**$^-$ charge recombination, represented by τ_2 and τ_3, could be expected as ALD of Al_2O_3 has been shown to be a means of slowing charge recombination in photoelectrodes, including our previously reported **PB6**-derivatized electrodes.[26,37,41] However, we do not observe a significant difference in the time components between the NiO-**PB6** and NiO-**PB6**-Al_2O_3 electrodes (Table 1). Since the Al_2O_3 layer is thinner (0.2 nm) than the optimized photocathodes in our prior work (1 nm),[42,46] it is likely the Al_2O_3 layer is too thin to significantly slow charge recombination. Regardless, as is seen in the decay associated spectra, we are still able to generate **PB6**$^-$ on the electrodes, which shows the potential to be used to reduce **Co** in the photocathode. Thus, in the photocathodes discussed here, Al_2O_3 simply serves as a surface to immobilize **Co** further from the NiO surface.

When the **L4** linker was added to the photocathodes in NiO-**PB6**-Al_2O_3-**L4**, transient absorption spectra similar to NiO-**PB6** were again observed (Figure S23). The decay associated spectra also clearly show the presence of the **PB6*** and **PB6**$^-$ species (Figure S24). With the alkyl chains surrounding **PB6** creating a hydrophobic environment, a slower NiO(+)−**PB6**$^-$ charge recombination would be expected.[24,35] Indeed, the third time component is lengthened from τ_3 = 3900 ps for NiO-**PB6**-Al_2O_3 to τ_3 = 5500 ps for NiO-**PB6**-Al_2O_3-**L4** (Table 1), suggesting that the alkyl linker helps slow charge recombination as hypothesized.

Finally, the effect of the **Co** catalyst was examined in NiO-**PB6**-Al_2O_3-**L4**-**Co** electrodes. Similar to the other photocathodes, the transient absorption spectra show the same features as NiO-**PB6** and the decay associated spectra suggest the formation of **PB6**$^-$ and **PB6*** on the electrode (Figures S23 and S24). The generation of **PB6**$^-$ on the catalyst-containing electrodes further supports that the electrodes function as expected. With **Co** present on the electrode, a faster τ_2 and/or τ_3 would be expected if **PB6**$^-$ can transfer an electron to **Co** on the surface, thereby bringing **PB6**$^-$ back to the ground state. In fact, we observe a shortening of τ_3 = 5500 ps for NiO-**PB6**-Al_2O_3-**L4** to τ_3 = 4600 ps for NiO-**PB6**-Al_2O_3-**L4**-**Co** (Table 1), suggesting that **PB6**$^-$ may reduce **Co** on the electrodes. In addition, kinetic traces at 620 nm show a smaller maximum signal in the presence of a catalyst. Recall from above that the traces at 620 nm show an initial negative signal (formation of **PB6***), which rises to a positive signal (formation of **PB6**$^-$) and decays to baseline (**PB6**$^-$ returns to the ground state); for further discussion of this, please see our previous work.[41] Since the positive max signal is smaller with the catalyst, this suggests faster decay of **PB6**$^-$ to the ground state, which could occur more rapidly if **PB6**$^-$ reduces a neighboring **Co** on the NiO surface. Thus, the traces at 620

https://dx.doi.org/10.1021/acsami.0c05228
ACS Appl. Mater. Interfaces 2020, 12, 31372−31381

nm also support that electron transfer to **Co** occurs on the ps time scale (Figure 5C). These results are similar to our previous study where we saw evidence for electron transfer from $PB6^-$ to a nickel complex on coimmobilized photocathodes using an identical analysis.[14]

H_2 Evolution. Furthermore, since NiO-**PB6**-Al_2O_3-**L4**-**Co** showed the best photocurrents and because we had evidence for electron transfer to **Co** by both photoelectrochemical measurements and fsTAS, H_2 evolution measurements were performed to see if catalytic proton reduction occurred. To do this, a Clark electrode was used to detect H_2; however, no significant H_2 was detected. If **Co** is not able to gain two reducing equivalents and two protons before charge recombination occurs, then this could result in a poor activity. However, we wondered if there could be other explanations for the inactivity. Recall that **Co** is active for electrocatalytic proton reduction in a MOF-immobilized electrode, hence we would expect that **Co** could be active for photoelectrocatalytic proton reduction when immobilized on the photocathodes.[54] Since we were not able to detect any H_2 when immobilized for photoelectrocatalysis, we wondered what may be happening on the electrode to limit performance.

Rationale for Electrode Performance. To understand the limitations of the electrode, stability measurements were performed. First, short-term stability was tested. To do this, chopped light CA was performed on the NiO-**PB6**-Al_2O_3-**L4**-**Co** electrodes over a 3 min period at 0.1 V vs NHE in 0.1 M MES buffer at pH 5. The electrodes were removed from the buffer, allowed to sit for 2 weeks in the dark, and then the CA was repeated (Figure S20). Remarkably, the majority of the photocurrent was retained, highlighting good short-term photostability. In addition, **Co** was still detected on the electrodes after CA by XRF measurements.

Since the electrodes appeared stable over the short term, longer 1 h CAs were performed. During these measurements, a large spike in photocurrent (hundreds of μAs) was observed that slowly decayed over the course of an hour, which reached less than 10 $\mu A/cm^2$ in 60 min (Figure S21). Clearly, the long-term stability of the electrodes is a limiting factor. UV−vis spectra of the electrode before and after the 1 h CA and of the electrolyte post CA show that the dye remains on the surface and does not appear to photodegrade or desorb, consistent with our prior results (Figure S9).[14] Since **PB6** was stable and did not limit the photocurrent, XRF measurements were performed to analyze the cobalt content on the electrode. To do this, XRF measurements were performed over 1 h, which display cobalt loss from the electrode over time, showing that about 80% of the initial cobalt was lost from the surface in 1 h (Figure 6). UV−vis spectra of the electrolyte during this time course also showed a new species growing over time, confirming that a species from the surface was desorbing into the electrolyte (Figure S10); the spectra does not match that of **Co** but could perhaps be a cobalt-containing salt or cobalt nanoparticles that form if the cobalt demetallates from the oxime ligand.[57] In addition, this new species is not present in the electrolyte if an identical CA experiment is performed with NiO-**PB6**-Al_2O_3-**L4** over 1 h, suggesting that the new UV−vis peak is likely from a cobalt species (Figure S11). Furthermore, **Co** remains bound to the electrode when it is soaked in 0.1 M MES buffer for 1 h, suggesting that the cobalt loss is only initiated when the samples are exposed to photoelectrochemical conditions. Cobaloxime degradation is not an unusual phenomenon, and specifically, cobalt

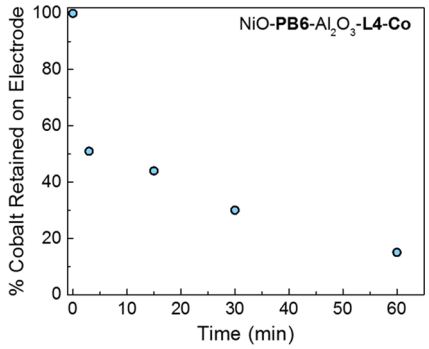

Figure 6. Percent cobalt retained on NiO-**PB6**-Al_2O_3-**L4**-**Co** during a 1 h CA under illumination with an applied bias of 0.1 V vs NHE in 0.1 M MES buffer at pH 5. XRF spectroscopic measurements were performed before and after CA to determine the percent cobalt retained on the electrode.

demetallation in cobaloxime complexes often occurs, as the reduced cobaloxime is known under certain conditions to be unstable when reduced in protic environments.[13,16,18,49,57−60] Finally, since cobalt is only lost under photoelectrochemical conditions on the photocathodes, this further supports that **Co** is reduced at least once on the electrode.

To obtain evidence for either cobalt demetallation or **Co** desorption, several experiments were performed. First, electrodes were prepared with a version of **L4**, but instead of a carboxylic acid anchor, a silatrane anchor was used (**L4Sil**, Figure S1). Silatranes are known to be stable anchor groups when bound to metal oxide surfaces under acidic, basic, and neutral conditions.[14,61−63] If **Co** was desorbing in the NiO-**PB6**-Al_2O_3-**L4**-**Co** electrode, the silatrane anchor should ensure that the whole catalyst remains bound to the surface in the NiO-**PB6**-Al_2O_3-**L4Sil**-**Co** electrodes. To test this, CA was performed for 1 h on the NiO-**PB6**-Al_2O_3-**L4Sil**-**Co** electrodes (see the SI for preparation details; Figure S22) and cobalt content analyzed before and after CA. Cobalt loss was still observed (50%), which suggests that cobalt was likely demetallating from the oxime ligand as **Co** desorption is less likely with a strong surface anchor. The amount of cobalt loss observed was slightly lower than with the carboxylic acid anchor (80% loss for the carboxylic acid anchor), which suggests that some **Co** from the NiO-**PB6**-Al_2O_3-**L4**-**Co** electrode may desorb, and the silatrane anchor can help stabilize **Co** desorption in the NiO-**PB6**-Al_2O_3-**L4Sil**-**Co** electrode.

Second, electrodes were prepared using ALD to further stabilize **Co**. ALD of TiO_2 has also been applied in various photoelectrode assemblies as a method to stabilize electrode constructs.[36,64−66] Specifically, ALD of TiO_2 has been shown to increase and stabilize photocurrents when used in $GaInP_2$-based photocathodes with cobaloxime catalysts.[67] In these electrodes, TiO_2 was applied over the cobalt catalyst under milder conditions at 150 °C.[67] By partially covering **Co** with TiO_2 on the electrode, **Co** desorption should not occur, similar to the electrodes containing silatrane-anchored **Co**. NiO-**PB6**-Al_2O_3-**L4**-**Co**-TiO_2 electrodes were prepared (see the SI for details) and CA performed for 1 h (Figure S22). Again, cobalt loss was observed by XRF (79% loss), suggesting that cobalt was demetallating from the oxime ligand rather than by simple desorption of the entire catalyst.

Furthermore, N 1s region XPS spectra of the NiO-**PB6**-Al_2O_3-**L4**-**Co** samples over time support that the majority of

https://dx.doi.org/10.1021/acsami.0c05228
ACS Appl. Mater. Interfaces 2020, 12, 31372−31381

the oxime ligand (400.4 eV, dashed line in Figure 7) may remain on the surface after 1 h of CA (Figure 7). A small

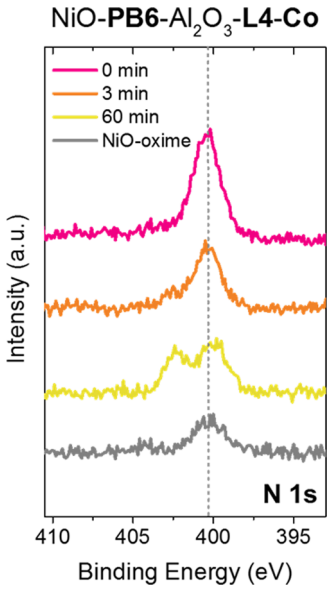

Figure 7. XPS spectra of the N 1s region of NiO-**PB6**-Al_2O_3-**L4**-**Co** (pink, 0 min). Photocathodes were illuminated for 3 min (orange) and 60 min (yellow) with a 0.1 V vs NHE bias in 0.1 M MES buffer at pH 5. A control sample with just the oxime ligand of **Co** bound to NiO is shown in gray (NiO-oxime). The NiO-oxime ligand electrode was prepared by soaking a NiO electrode in a 0.1 mM oxime ligand (structure shown in Figure S14) methanol solution for 2 h, rinsed with methanol, and air-dried.

decrease in the N 1s intensity is initially observed, suggesting that some **Co** desorption may occur, consistent with the above results using the silatrane anchor (NiO-**PB6**-Al_2O_3-**L4Sil**-**Co**). Alternatively, if cobalt demetallates from the oxime ligand, one of the two oxime ligands coordinated to cobalt should be lost, while the other remains surface-immobilized; this could also lower the N 1s intensity. During 1 h of CA, an additional peak appears over time (402.1 eV) and some broadening of the oxime ligand peak is observed, which is likely due to the MES buffer adsorbing on the electrode (Figure S15). MES buffer shows two signals in the N 1s region at 402.1 and 399.4 eV (Figure S15). When the XPS spectra are overlaid and examined, the spectrum of NiO-**PB6**-Al_2O_3-**L4**-**Co** at 60 min appears to have both oxime ligand and MES components (Figure S15); additional XPS analysis of this can be found in the SI. In addition, cobalt loss is still observed when no linker is present on the surface post CA (NiO-**PB6**-Al_2O_3-**Co**) with the majority of the oxime ligand remaining on the electrode; this further suggests that cobalt loss does not result from the use of alkyl linkers but is an inherent instability when surface-bound to the photocathode under photoelectrochemical conditions (Figure S16). Therefore, based on the XPS data, it appears that the majority of the oxime ligand remains on the photocathode after 1 h of electrolysis, supporting that mainly cobalt demetallation occurs on the electrode. Additional XPS data can be found in the SI. Taken together, the UV−vis data, XRF data, silatrane alkyl linker control experiments, ALD of TiO_2 over **Co**, and the XPS data support that cobalt demetallation from the oxime ligand is likely the main deactivation pathway of these electrodes.

Overall, based on evidence from the photoelectrochemical results, fsTAS results, and the observed cobalt loss from the photocathodes, **Co** can be reduced at least once on the photocathodes. Since cobaloxime reduction is known to cause catalyst instability, the reduction of **Co** likely contributes to limiting the photocathode performance by causing cobalt demetallation.

Furthermore, **Co** has also been shown to be electrocatalytically active for homogeneous proton reduction catalysis under aqueous conditions at pH 5.3, producing 15.2 μmol H_2 with a 90% Faradaic yield.[54] However, the stability of **Co** under homogenous electrocatalytic conditions has not been analyzed. Specifically, it remains unknown whether the homogenous analogue degrades, and if it does, how—possibly via demetallation, ligand degradation, or nanoparticle formation. As degradation under homogenous conditions has been observed with many other cobaloxime catalysts, this possibility remains likely.[57] As we have explored cobalt demetallation and ligand changes above, this leaves nanoparticle formation to still be considered. Since nanoparticles are usually active for proton reduction catalysis and we do not see any H_2 evolved from our system, we likely do not have significant nanoparticle formation on the photocathodes studied here. Thus, cobalt demetallation remains the most likely reason for low photocathode performance.

Clearly, the catalyst's surrounding environment plays a role in its stability, as **Co** was stable and catalytically active when immobilized in a MOF.[54] The MOF structure may act as a protecting environment by keeping the cobalt metal in a secure binding site upon reduction, where the oxime-coordinated cobalt is held in the MOF by all four carboxylic acids on the oxime ligands in a rigid, locked, enclosed architecture. Conversely, on the photocathodes, **Co** is in a less rigid or contained environment, being attached to the metal oxide surface via carboxylic acid anchoring groups on the oxime ligand or alkyl linkers. In addition, in this architecture, **Co** likely has greater exposure to the surrounding electrolyte than in the enclosed MOF structure, providing an easier way for the cobalt to demetallate. Without alkyl linkers, **Co** is likely bound to the photocathode surface by one or two of the carboxylic acid anchors on the oxime ligands, which results in a less rigid surface binding than in the MOF, which had all four carboxylic acids securing the catalyst. The less rigid environment likely contributes to instability of these electrodes, promoting cobalt loss by having more conformational freedom. In the photocathodes with alkyl linkers, the cobalt is coordinated to oxime ligands with flexible alkyl linkers, and in this architecture, **Co** has more conformational freedom due to the flexible alkyl chains, which could upon photoreduction encourage the release of the cobalt center, which then travels into the bulk electrolyte.

Electrochemically driven catalysis in the MOF is perhaps simpler than photoelectrocatalysis on a photocathode as the reducing equivalents are provided via electron hopping from the conductive electrode to **Co**, whereas, in the photocathode, charge must accumulate at **Co** after **PB6** excitation, hole injection, and electron transfer to **Co** twice. Since there are more steps to accumulate charge at **Co**, which takes more time, there are more opportunities for charge recombination, which makes accumulating two reducing equivalents at **Co** more challenging. In the photocathodes studied here, there is an additional challenge as the reduction of **Co** likely causes cobalt demetallation and photocathode deactivation. Therefore, if the

https://dx.doi.org/10.1021/acsami.0c05228
ACS Appl. Mater. Interfaces 2020, 12, 31372−31381

cobalt metal center is removed from the ligand, charge accumulation will not occur at the catalyst since it no longer remains intact, which then lowers the overall performance of these electrodes.

CONCLUSIONS

Here, we have prepared photocathodes containing **PB6** dye and alkyl-linked cobalt catalysts. The use of linkers led to higher photocurrents compared to when catalysts were linked directly on the electrode. An intriguing photocurrent dependence on the linker length of **Co** was found via photoelectrochemical measurements with the **L4** linker showing highest photocurrents followed by a current drop-off with longer linkers, which separate **Co** further from **PB6**. In our system, the **L4** linker provided the optimal height for the **Co** catalyst with respect to **PB6** and NiO, showing the largest photocurrents reproducibly. Ultrafast electron transfer dynamics suggested that the alkyl linkers slowed NiO−**PB6** charge recombination, while ALD had little effect, likely due to the layer being too thin. Evidence for electron transfer to **Co** by **PB6**$^-$ was supported by photoelectrochemical experiments and the fs-transient absorption studies. Since **Co** was likely reduced by **PB6**$^-$ at least once on the electrodes, the best samples were tested for H_2 evolution, but no H_2 was detected. To understand this, several control experiments were performed that suggested the dominating pathway for photocathode deactivation was via cobalt demetallation from the oxime ligand, leading to a loss in photocurrent and catalysis. Based on these results, to make improvements in photocathode performance, molecular design of catalysts specifically for surface-immobilized photoelectrocatalysis must absolutely be considered in photocathode design. Of course, slowing charge recombination is also important to consider, but if the catalyst becomes deactivated by not having an optimal molecular structure, then there is no chance for the charge to build up at the catalyst. Thus, one should always consider that catalysts used for electrocatalysis may not always be a suitable choice for photoelectrocatalysis as the mechanisms and timescales for charge accumulation are different.

ASSOCIATED CONTENT

Supporting Information

The Supporting Information is available free of charge at https://pubs.acs.org/doi/10.1021/acsami.0c05228.

> Experimental details such as the preparation method of the octanoic acid and **L4Sil**-containing photocathodes, preparation of the control sample using TiO_2 ALD, and further details of the preparation of the **L4**, **L8**, and **L11**-containing photocathodes can be found in the SI. Further experimental data such as UV−vis, ATR-FTIR, XPS, fsTAS, XRF calibration curve, and dye and catalyst loadings can also be found in the SI (PDF)

AUTHOR INFORMATION

Corresponding Author

Leif Hammarström − *Department of Chemistry-Ångström Laboratories, Uppsala University, SE75120 Uppsala, Sweden;* orcid.org/0000-0002-9933-9084; Email: leif.hammarstrom@kemi.uu.se

Authors

Kelly L. Materna − *Department of Chemistry-Ångström Laboratories, Uppsala University, SE75120 Uppsala, Sweden*

Anna M. Beiler − *Department of Chemistry-Ångström Laboratories, Uppsala University, SE75120 Uppsala, Sweden*

Anders Thapper − *Department of Chemistry-Ångström Laboratories, Uppsala University, SE75120 Uppsala, Sweden;* orcid.org/0000-0001-7643-302X

Sascha Ott − *Department of Chemistry-Ångström Laboratories, Uppsala University, SE75120 Uppsala, Sweden;* orcid.org/0000-0002-1691-729X

Haining Tian − *Department of Chemistry-Ångström Laboratories, Uppsala University, SE75120 Uppsala, Sweden;* orcid.org/0000-0001-6897-2808

Complete contact information is available at: https://pubs.acs.org/10.1021/acsami.0c05228

Notes

The authors declare no competing financial interest.

ACKNOWLEDGMENTS

We thank the Swedish Energy Agency (Grant no. 11674-8) for funding this research. A.M.B. was supported by the Olle Engkvist Byggmästare Foundation. We also thank Belinda Pettersson Rimgard for help in collecting the fsTAS data and aid in learning data analysis. We thank Dr. Brian McCarthy for help in editing the text and scientific input. We thank Dr. Bo Xu for making the NiO screen-printing paste, Dr. Palas Baran Pati for synthesizing **PB6**, Dr. Souvik Roy for synthesizing **Co**, and Dr. Jens Föhlinger and Jonas Petterson for writing the MATLAB script for global fitting.

REFERENCES

(1) Outlook EA. *Annual Energy*; EIA: Washington, DC, USA, 2017.

(2) Wang, Y.; Suzuki, H.; Xie, J.; Tomita, O.; Martin, D. J.; Higashi, M.; Kong, D.; Abe, R.; Tang, J. Mimicking Natural Photosynthesis: Solar to Renewable H2 Fuel Synthesis by Z-Scheme Water Splitting Systems. *Chem. Rev.* **2018**, *118*, 5201−5241.

(3) Brennaman, M. K.; Dillon, R. J.; Alibabaei, L.; Gish, M. K.; Dares, C. J.; Ashford, D. L.; House, R. L.; Meyer, G. J.; Papanikolas, J. M.; Meyer, T. J. Finding the Way to Solar Fuels with Dye-Sensitized Photoelectrosynthesis Cells. *J. Am. Chem. Soc.* **2016**, 13085−13102.

(4) Yu, Z.; Li, F.; Sun, L. Recent Advances in Dye-Sensitized Photoelectrochemical Cells for Solar Hydrogen Production Based on Molecular Components. *Energy Environ. Sci.* **2015**, *8*, 760−775.

(5) Swierk, J. R.; Mallouk, T. E. Design and Development of Photoanodes for Water-Splitting Dye-Sensitized Photoelectrochemical Cells. *Chem. Soc. Rev.* **2013**, *42*, 2357−2387.

(6) Ashford, D. L.; Gish, M. K.; Vannucci, A. K.; Brennaman, M. K.; Templeton, J. L.; Papanikolas, J. M.; Meyer, T. J. Molecular Chromophore-Catalyst Assemblies for Solar Fuel Applications. *Chem. Rev.* **2015**, *115*, 13006−13049.

(7) Tian, H. Molecular Catalyst Immobilized Photocathodes for Water/Proton and Carbon Dioxide Reduction. *ChemSusChem* **2015**, *8*, 3746−3759.

(8) Gibson, E. A. Dye-Sensitized Photocathodes for H2 Evolution. *Chem. Soc. Rev.* **2017**, *46*, 6194−6209.

(9) Wood, C. J.; Summers, G. H.; Clark, C. A.; Kaeffer, N.; Braeutigam, M.; Carbone, L. R.; D'Amario, L.; Fan, K.; Farre, Y.; Narbey, S.; Oswald, F.; Stevens, L. A.; Parmenter, C. D.; Fay, M. W.; La Torre, A.; Snape, C. E.; Dietzek, B.; Dini, D.; Hammarstrom, L.; Pellegrin, Y.; Odobel, F.; Sun, L.; Artero, V.; Gibson, E. A. A Comprehensive Comparison of Dye-Sensitized Nio Photocathodes for Solar Energy Conversion. *Phys. Chem. Chem. Phys.* **2016**, *18*, 10727−10738.

(10) Fan, K.; Li, F.; Wang, L.; Daniel, Q.; Gabrielsson, E.; Sun, L. Pt-Free Tandem Molecular Photoelectrochemical Cells for Water Splitting Driven by Visible Light. *Phys. Chem. Chem. Phys.* **2014**, *16*, 25234−25240.
(11) Li, F.; Fan, K.; Xu, B.; Gabrielsson, E.; Daniel, Q.; Li, L.; Sun, L. Organic Dye-Sensitized Tandem Photoelectrochemical Cell for Light Driven Total Water Splitting. *J. Am. Chem. Soc.* **2015**, *137*, 9153−9159.
(12) Antila, L. J.; Ghamgosar, P.; Maji, S.; Tian, H.; Ott, S.; Hammarström, L. Dynamics and Photochemical H2 Evolution of Dye−Nio Photocathodes with a Biomimetic Fefe-Catalyst. *ACS Energy Lett.* **2016**, *1*, 1106−1111.
(13) Kaeffer, N.; Windle, C. D.; Brisse, R.; Gablin, C.; Leonard, D.; Jousselme, B.; Chavarot-Kerlidou, M.; Artero, V. Insights into the Mechanism and Aging of a Noble-Metal Free H2-Evolving Dye-Sensitized Photocathode. *Chem. Sci.* **2018**, *9*, 6721−6738.
(14) Materna, K. L.; Lalaoui, N.; Laureanti, J. A.; Walsh, A. P.; Rimgard, B. P.; Lomoth, R.; Thapper, A.; Ott, S.; Shaw, W. J.; Tian, H.; Hammarstrom, L. Using Surface Amide Couplings to Assemble Photocathodes for Solar Fuel Production Applications. *ACS Appl. Mater. Interfaces* **2020**, *12*, 4501−4509.
(15) van den Bosch, B.; Rombouts, J. A.; Orru, R. V. A.; Reek, J. N. H.; Detz, R. J. Nickel-Based Dye-Sensitized Photocathode: Towards Proton Reduction Using a Molecular Nickel Catalyst and an Organic Dye. *ChemCatChem* **2016**, *8*, 1392−1398.
(16) Windle, C. D.; Kumagai, H.; Higashi, M.; Brisse, R.; Bold, S.; Jousselme, B.; Chavarot-Kerlidou, M.; Maeda, K.; Abe, R.; Ishitani, O.; Artero, V. Earth-Abundant Molecular Z-Scheme Photoelectrochemical Cell for Overall Water-Splitting. *J. Am. Chem. Soc.* **2019**, *141*, 9593−9602.
(17) Lyu, S.; Massin, J.; Pavone, M.; Muñoz-García, A. B.; Labrugère, C.; Toupance, T.; Chavarot-Kerlidou, M.; Artero, V.; Olivier, C. H2-Evolving Dye-Sensitized Photocathode Based on a Ruthenium−Diacetylide/Cobaloxime Supramolecular Assembly. *ACS Appl. Energy Mater.* **2019**, *2*, 4971−4980.
(18) Pati, P. B.; Zhang, L.; Philippe, B.; Fernandez-Teran, R.; Ahmadi, S.; Tian, L.; Rensmo, H.; Hammarstrom, L.; Tian, H. Insights into the Mechanism of a Covalently Linked Organic Dye-Cobaloxime Catalyst System for Dye-Sensitized Solar Fuel Devices. *ChemSusChem* **2017**, *10*, 2480−2495.
(19) Põldme, N.; O'Reilly, L.; Fletcher, I.; Portoles, J.; Sazanovich, I. V.; Towrie, M.; Long, C.; Vos, J. G.; Pryce, M. T.; Gibson, E. A. Photoelectrocatalytic H2 Evolution from Integrated Photocatalysts Adsorbed on Nio. *Chem. Sci.* **2019**, *10*, 99−112.
(20) Windle, C. D.; Massin, J.; Chavarot-Kerlidou, M.; Artero, V. A Protocol for Quantifying Hydrogen Evolution by Dye-Sensitized Molecular Photocathodes and Its Implementation for Evaluating a New Covalent Architecture Based on an Optimized Dye-Catalyst Dyad. *Dalton Trans.* **2018**, *47*, 10509−10516.
(21) Gross, M. A.; Creissen, C. E.; Orchard, K. L.; Reisner, E. Photoelectrochemical Hydrogen Production in Water Using a Layer-by-Layer Assembly of a Ru Dye and Ni Catalyst on Nio. *Chem. Sci.* **2016**, *7*, 5537−5546.
(22) Shan, B.; Nayak, A.; Brennaman, M. K.; Liu, M.; Marquard, S. L.; Eberhart, M. S.; Meyer, T. J. Controlling Vertical and Lateral Electron Migration Using a Bifunctional Chromophore Assembly in Dye-Sensitized Photoelectrosynthesis Cells. *J. Am. Chem. Soc.* **2018**, *140*, 6493−6500.
(23) Shan, B.; Sherman, B. D.; Klug, C. M.; Nayak, A.; Marquard, S. L.; Liu, Q.; Bullock, R. M.; Meyer, T. J. Modulating Hole Transport in Multilayered Photocathodes with Derivatized P-Type Nickel Oxide and Molecular Assemblies for Solar-Driven Water Splitting. *J. Phys. Chem. Lett.* **2017**, *8*, 4374−4379.
(24) Click, K. A.; Beauchamp, D. R.; Huang, Z.; Chen, W.; Wu, Y. Membrane-Inspired Acidically Stable Dye-Sensitized Photocathode for Solar Fuel Production. *J. Am. Chem. Soc.* **2016**, *138*, 1174−1179.
(25) Xu, B.; Tian, L.; Etman, A. S.; Sun, J.; Tian, H. Solution-Processed Nanoporous Nio-Dye-Zno Photocathodes: Toward Efficient and Stable Solid-State P-Type Dye-Sensitized Solar Cells and Dye-Sensitized Photoelectrosynthesis Cells. *Nano Energy* **2019**, *55*, 59−64.
(26) Kamire, R. J.; Majewski, M. B.; Hoffeditz, W. L.; Phelan, B. T.; Farha, O. K.; Hupp, J. T.; Wasielewski, M. R. Photodriven Hydrogen Evolution by Molecular Catalysts Using Al2o3-Protected Perylene-3,4-Dicarboximide on Nio Electrodes. *Chem. Sci.* **2017**, *8*, 541−549.
(27) Shan, B.; Nayak, A.; N. Sampaio, R.; Eberhart, M. S.; Troian-Gautier, L.; Brennaman, M. K.; Meyer, G. J.; Meyer, T. J. Direct Photoactivation of a Nickel-Based, Water-Reduction Photocathode by a Highly Conjugated Supramolecular Chromophore. *Energy Environ. Sci.* **2018**, *11*, 447−455.
(28) Daeneke, T.; Yu, Z.; Lee, G. P.; Fu, D. C.; Duffy, N. W.; Makuta, S.; Tachibana, Y.; Spiccia, L.; Mishra, A.; Baeuerle, P.; Bach, U. Dominating Energy Losses in Nio P-Type Dye-Sensitized Solar Cells. *Adv. Energy Mater.* **2015**, *5*, No. 1401387.
(29) D'Amario, L.; Antila, L. J.; Pettersson Rimgard, B.; Boschloo, G.; Hammarstrom, L. Kinetic Evidence of Two Pathways for Charge Recombination in Nio-Based Dye-Sensitized Solar Cells. *J. Phys. Chem. Lett.* **2015**, *6*, 779−783.
(30) D'Amario, L.; Föhlinger, J.; Boschloo, G.; Hammarström, L. Unveiling Hole Trapping and Surface Dynamics of Nio Nanoparticles. *Chem. Sci.* **2018**, *9*, 223−230.
(31) D'Amario, L.; Jiang, R.; Cappel, U. B.; Gibson, E. A.; Boschloo, G.; Rensmo, H.; Sun, L.; Hammarstrom, L.; Tian, H. Chemical and Physical Reduction of High Valence Ni States in Mesoporous Nio Film for Solar Cell Application. *ACS Appl. Mater. Interfaces* **2017**, *9*, 33470−33477.
(32) Morandeira, A.; Boschloo, G.; Hagfeldt, A.; Hammarstrom, L. Photoinduced Ultrafast Dynamics of Coumarin 343 Sensitized P-Type-Nanostructured Nio Films. *J. Phys. Chem. B* **2005**, *109*, 19403−19410.
(33) Morandeira, A.; Boschloo, G.; Hagfeldt, A.; Hammarström, L. Coumarin 343-Nio Films as Nanostructured Photocathodes in Dye-Sensitized Solar Cells: Ultrafast Electron Transfer, Effect of the $I3^-/I^-$ Redox Couple and Mechanism of Photocurrent Generation. *J. Phys. Chem. C* **2008**, *112*, 9530−9537.
(34) Mori, S.; Fukuda, S.; Sumikura, S.; Takeda, Y.; Tamaki, Y.; Suzuki, E.; Abe, T. Charge-Transfer Processes in Dye-Sensitized Nio Solar Cells. *J. Phys. Chem. C* **2008**, *112*, 16134−16139.
(35) Kroeze, J. E.; Hirata, N.; Koops, S.; Nazeeruddin, M. K.; Schmidt-Mende, L.; Gratzel, M.; Durrant, J. R. Alkyl Chain Barriers for Kinetic Optimization in Dye-Sensitized Solar Cells. *J. Am. Chem. Soc.* **2006**, *128*, 16376−16383.
(36) Lapides, A. M.; Sherman, B. D.; Brennaman, K.; Dares, C. J.; Skinner, K. R.; Templeton, J.; Meyer, T. J. Synthesis, Characterization, and Water Oxidation by a Molecular Chromophore-Catalyst Assembly Prepared by Atomic Layer Deposition. The "Mummy" Strategy. *Chem. Sci.* **2015**, *6*, 6398−6406.
(37) Natu, G.; Huang, Z.; Ji, Z.; Wu, Y. The Effect of an Atomically Deposited Layer of Alumina on Nio in P-Type Dye-Sensitized Solar Cells. *Langmuir* **2012**, *28*, 950−956.
(38) Prasittichai, C.; Avila, J. R.; Farha, O. K.; Hupp, J. T. Systematic Modulation of Quantum (Electron) Tunneling Behavior by Atomic Layer Deposition on Nanoparticulate Sno2 and Tio2 Photoanodes. *J. Am. Chem. Soc.* **2013**, *135*, 16328−16331.
(39) Hanson, K.; Losego, M. D.; Kalanyan, B.; Ashford, D. L.; Parsons, G. N.; Meyer, T. J. Stabilization of [Ru(Bpy)2(4,4′-(Po3h2)Bpy)]2+ on Mesoporous Tio2 with Atomic Layer Deposition of Al2o3. *Chem. Mater.* **2012**, *25*, 3−5.
(40) Ji, Z.; He, M.; Huang, Z.; Ozkan, U.; Wu, Y. Photostable P-Type Dye-Sensitized Photoelectrochemical Cells for Water Reduction. *J. Am. Chem. Soc.* **2013**, *135*, 11696−11699.
(41) Tian, L.; Fohlinger, J.; Pati, P. B.; Zhang, Z.; Lin, J.; Yang, W.; Johansson, M.; Kubart, T.; Sun, J.; Boschloo, G.; Hammarstrom, L.; Tian, H. Ultrafast Dye Regeneration in a Core-Shell Nio-Dye-Tio2 Mesoporous Film. *Phys. Chem. Chem. Phys.* **2017**, *20*, 36−40.
(42) Tian, L.; Fohlinger, J.; Zhang, Z.; Pati, P. B.; Lin, J.; Kubart, T.; Hua, Y.; Sun, J.; Kloo, L.; Boschloo, G.; Hammarstrom, L.; Tian, H.

https://dx.doi.org/10.1021/acsami.0c05228
ACS Appl. Mater. Interfaces 2020, 12, 31372−31381

Solid State P-Type Dye Sensitized Nio-Dye-Tio2 Core-Shell Solar Cells. *Chem. Commun.* **2018**, *54*, 3739−3742.
(43) Dempsey, J. L.; Brunschwig, B. S.; Winkler, J. R.; Gray, H. B. Hydrogen Evolution Catalyzed by Cobaloximes. *Acc. Chem. Res.* **2009**, *42*, 1995−2004.
(44) Kamire, R. J.; Materna, K. L.; Hoffeditz, W. L.; Phelan, B. T.; Thomsen, J. M.; Farha, O. K.; Hupp, J. T.; Brudvig, G. W.; Wasielewski, M. R. Photodriven Oxidation of Surface-Bound Iridium-Based Molecular Water-Oxidation Catalysts on Perylene-3,4-Dicarboximide-Sensitized Tio2 Electrodes Protected by an Al2o3 Layer. *J. Phys. Chem. C* **2017**, *121*, 3752−3764.
(45) Hanson, K.; Losego, M. D.; Kalanyan, B.; Parsons, G. N.; Meyer, T. J. Stabilizing Small Molecules on Metal Oxide Surfaces Using Atomic Layer Deposition. *Nano Lett.* **2013**, *13*, 4802−4809.
(46) DuBois, D. L.; Bullock, R. M. Molecular Electrocatalysts for the Oxidation of Hydrogen and the Production of Hydrogen—the Role of Pendant Amines as Proton Relays. *Eur. J. Inorg. Chem.* **2011**, *2011*, 1017−1027.
(47) Baffert, C.; Artero, V.; Fontecave, M. Cobaloximes as Functional Models for Hydrogenases. 2. Proton Electroreduction Catalyzed by Difluoroborylbis(Dimethylglyoximato)Cobalt(Ii) Complexes in Organic Media. *Inorg. Chem.* **2007**, *46*, 1817−1824.
(48) Jacques, P. A.; Artero, V.; Pecaut, J.; Fontecave, M. Cobalt and Nickel Diimine-Dioxime Complexes as Molecular Electrocatalysts for Hydrogen Evolution with Low Overvoltages. *Proc. Natl. Acad. Sci. U.S.A.* **2009**, *106*, 20627−20632.
(49) Kaeffer, N.; Chavarot-Kerlidou, M.; Artero, V. Hydrogen Evolution Catalyzed by Cobalt Diimine-Dioxime Complexes. *Acc. Chem. Res.* **2015**, *48*, 1286−1295.
(50) Kaeffer, N.; Massin, J.; Lebrun, C.; Renault, O.; Chavarot-Kerlidou, M.; Artero, V. Covalent Design for Dye-Sensitized H2-Evolving Photocathodes Based on a Cobalt Diimine-Dioxime Catalyst. *J. Am. Chem. Soc.* **2016**, *138*, 12308−12311.
(51) Lakadamyali, F.; Reisner, E. Photocatalytic H2 Evolution from Neutral Water with a Molecular Cobalt Catalyst on a Dye-Sensitised Tio2 Nanoparticle. *Chem. Commun.* **2011**, *47*, 1695−1697.
(52) Li, L.; Duan, L.; Wen, F.; Li, C.; Wang, M.; Hagfeldt, A.; Sun, L. Visible Light Driven Hydrogen Production from a Photo-Active Cathode Based on a Molecular Catalyst and Organic Dye-Sensitized P-Type Nanostructured Nio. *Chem. Commun.* **2012**, *48*, 988−990.
(53) Willkomm, J.; Muresan, N. M.; Reisner, E. Enhancing H2 Evolution Performance of an Immobilised Cobalt Catalyst by Rational Ligand Design. *Chem. Sci.* **2015**, *6*, 2727−2736.
(54) Roy, S.; Huang, Z.; Bhunia, A.; Castner, A.; Gupta, A. K.; Zou, X.; Ott, S. Electrocatalytic Hydrogen Evolution from a Cobaloxime-Based Metal-Organic Framework Thin Film. *J. Am. Chem. Soc.* **2019**, *141*, 15942−15950.
(55) Beiler, A. M.; Khusnutdinova, D.; Jacob, S. I.; Moore, G. F. Solar Hydrogen Production Using Molecular Catalysts Immobilized on Gallium Phosphide (111)a and (111)B Polymer-Modified Photocathodes. *ACS Appl. Mater. Interfaces* **2016**, *8*, 10038−10047.
(56) Zhang, L.; Boschloo, G.; Hammarstrom, L.; Tian, H. Solid State P-Type Dye-Sensitized Solar Cells: Concept, Experiment and Mechanism. *Phys. Chem. Chem. Phys.* **2016**, *18*, 5080−5085.
(57) Lee, K. J.; McCarthy, B. D.; Dempsey, J. L. On Decomposition, Degradation, and Voltammetric Deviation: The Electrochemist's Field Guide to Identifying Precatalyst Transformation. *Chem. Soc. Rev.* **2019**, *48*, 2927−2945.
(58) Kaeffer, N.; Morozan, A.; Fize, J.; Martinez, E.; Guetaz, L.; Artero, V. The Dark Side of Molecular Catalysis: Diimine−Dioxime Cobalt Complexes Are Not the Actual Hydrogen Evolution Electrocatalyst in Acidic Aqueous Solutions. *ACS Catal.* **2016**, *6*, 3727−3737.
(59) Anxolabéhère-Mallart, E.; Costentin, C.; Fournier, M.; Robert, M. Cobalt-Bisglyoximato Diphenyl Complex as a Precatalyst for Electrocatalytic H2evolution. *J. Phys. Chem. C* **2014**, *118*, 13377−13381.
(60) Baxter, L. A.; Bobrowski, A.; Bond, A. M.; Heath, G. A.; Paul, R. L.; Mrzljak, R.; Zarebski, J. Electrochemical and Spectroscopic Investigation of the Reduction of Dimethylglyoxime at Mercury Electrodes in the Presence of Cobalt and Nickel. *Anal. Chem.* **1998**, *70*, 1312−1323.
(61) Materna, K. L.; Brennan, B. J.; Brudvig, G. W. Silatranes for Binding Inorganic Complexes to Metal Oxide Surfaces. *Dalton Trans.* **2015**, *44*, 20312−20315.
(62) Materna, K. L.; Crabtree, R. H.; Brudvig, G. W. Anchoring Groups for Photocatalytic Water Oxidation on Metal Oxide Surfaces. *Chem. Soc. Rev.* **2017**, *46*, 6099−6110.
(63) Materna, K. L.; Jiang, J.; Crabtree, R. H.; Brudvig, G. W. Silatrane Anchors for Metal Oxide Surfaces: Optimization for Potential Photocatalytic and Electrocatalytic Applications. *ACS Appl. Mater. Interfaces* **2019**, *11*, 5602−5609.
(64) Alibabaei, L.; Sherman, B. D.; Norris, M. R.; Brennaman, M. K.; Meyer, T. J. Visible Photoelectrochemical Water Splitting into H2 and O2 in a Dye-Sensitized Photoelectrosynthesis Cell. *Proc. Natl. Acad. Sci. U.S.A.* **2015**, *112*, 5899−5902.
(65) Chandrasekaran, S.; Kaeffer, N.; Cagnon, L.; Aldakov, D.; Fize, J.; Nonglaton, G.; Baleras, F.; Mailley, P.; Artero, V. A Robust Ald-Protected Silicon-Based Hybrid Photoelectrode for Hydrogen Evolution under Aqueous Conditions. *Chem. Sci.* **2019**, *10*, 4469−4475.
(66) Nam, D. H.; Zhang, J. Z.; Andrei, V.; Kornienko, N.; Heidary, N.; Wagner, A.; Nakanishi, K.; Sokol, K. P.; Slater, B.; Zebger, I.; Hofmann, S.; Fontecilla-Camps, J. C.; Park, C. B.; Reisner, E. Solar Water Splitting with a Hydrogenase Integrated in Photoelectrochemical Tandem Cells. *Angew. Chem., Int. Ed.* **2018**, *57*, 10595−10599.
(67) Gu, J.; Yan, Y.; Young, J. L.; Steirer, K. X.; Neale, N. R.; Turner, J. A. Water Reduction by a P-Gainp2 Photoelectrode Stabilized by an Amorphous Tio2 Coating and a Molecular Cobalt Catalyst. *Nat. Mater.* **2016**, *15*, 456−460.

https://dx.doi.org/10.1021/acsami.0c05228
ACS Appl. Mater. Interfaces 2020, 12, 31372−31381